H 2 -Evolving Dye-Sensitized Photocathode Based on a Ruthenium Diacetylide/Cobaloxime Supramolecular Assembly

Siliu Lyu, Julien Massin, Michéle Pavone, Ana Muñoz-García, Christine Labrugère, Thierry Toupance, Murielle Chavarot-Kerlidou, Vincent Artero, Céline Olivier

H₂-Evolving Dye-Sensitized Photocathode Based on a Ruthenium Diacetylide/Cobaloxime Supramolecular Assembly

Siliu Lyu (1), Julien Massin (2), Michele Pavone (3), Ana B. Muñoz-García (4), Christine Labrugère (5), Thierry Toupance (1), Murielle Chavarot-Kerlidou (2), Vincent Artero (2),* Céline Olivier (1)*

(1) Institut des Sciences Moléculaires, Univ. Bordeaux, CNRS UMR 5255, Talence, France.

(2) Univ. Grenoble Alpes, CNRS, CEA, LCBM, 38000 Grenoble, France.

(3) University of Naples Federico II, Department of Chemical Sciences, Via Cintia 21, 80126 Napoli, Italy.

(4) University of Naples Federico II, Department of Physics "E. Pancini", Via Cintia 21, 80126 Napoli, Italy.

(5) PLACAMAT, Univ. Bordeaux, CNRS, UMS 3626, Pessac, France.

KEYWORDS. Molecular photocatalyst; Dye-sensitized photoelectrochemical cell; Nickel oxide; Ruthenium diacetylide complex; Cobaloxime.

ABSTRACT

The development of NiO-based molecular photocathodes is attracting growing interest in the field of dye-sensitized photoelectrochemical cells (DS-PEC) for efficient conversion of sunlight into fuel. For this purpose different strategies are developed to assemble the molecular components together in order to build functional devices. Here, an original dye-catalyst supramolecular assembly was designed and obtained via axial coordination of a cobalt-based H_2-evolving catalyst, *i.e.* a cobaloxime complex, to a pyridyl-functionalized ruthenium-diacetylide photosensitizer. The new supramolecular assembly was successfully employed for the construction of efficient NiO-based photocathodes for solar hydrogen production. We report a joint experimental and theoretical study of the new photocatalytic system, including electrochemical and XPS analyses. Photo-electrochemical generation of H_2 under pertinent aqueous conditions eventually led to a faradaic efficiency of 27 %.

INTRODUCTION

The development of renewable energies is a major issue to be addressed in response to the problem of profuse and environmentally friendly energy for large-scale sustainable development. A realistic energy conversion method is the use of efficient photo(electro)catalytic systems that can convert the energy of the sun into storable chemical fuels, typically by splitting water into oxygen and hydrogen.[1, 2] In particular, hydrogen presents many advantages of being produced and used as a 'solar fuel',[3, 4] *e.g.* it presents a high heat of combustion and can be used on demand in fuel cells that produce a harmless combustion by-product, that is water.[5] Moreover, the use of hydrogen limits the one of fossil fuels and subsequent emissions of greenhouse gases. All these reasons have been a strong incentive for the development of efficient homogeneous systems able to convert solar energy and water into hydrogen. These photocatalytic systems typically rely on dye/catalyst molecular assemblies in association with a sacrificial electron donor (SED) such as triethylamine (TEA) or triethanolamine (TEOA) in mixed organic/aqueous solutions.[6-9] Here it is worth mentioning that efficient H_2-evolving molecular catalysts are mostly based on cobalt complexes or other earth-abundant metals like nickel or iron.[10-13] In particular, cobaloximes proved to be candidates of choice for both efficiency and stability reasons.[6-9, 14, 15]

More recently, molecular dyes and catalysts were grafted onto wide band gap semiconductors in order to build dye-sensitized photoelectrochemical cells (DS-PEC) for efficient conversion of sunlight into fuel.[16-20] The development of NiO-based photocathodes sparks growing interest in this field[21-23] and different strategies were reported to assemble the molecular components together in order to build functional devices; these are typically dye-sensitized photocathodes combined with a catalyst in solution,[24-26] co-grafted dye/catalyst systems,[27-31] layer-by-layer assemblies of the dye and the catalyst[32-35] and finally covalent or supramolecular dye/catalyst assemblies onto the electrode.[36-38] In the latter case, an attractive construction involves axial coordination of a pyridyl-substituted dye to a cobaloxime

catalyst.[36] This strategy was first reported by one of us for homogeneous hydrogen production by related cobaloxime-based supramolecular photocatalytic assemblies.[6,7] As far as the dye is concerned, two families of light-harvesting units are mainly used: organic push-pull chromophores and ruthenium tris-bipyridine derivatives. Recently, we demonstrated the relevance of using original push-pull ruthenium-diacetylide complexes as photosensitizers in NiO-based photocathodes for p-type dye-sensitized solar cells and photo-electrochemical cells.[39, 40] Ruthenium-diacetylide are neutral complexes featuring a linear π-conjugated system that are used as versatile tools for the preparation of push-pull chromophores with valuable optical and electronic properties. Here we report the design and synthesis of a new dye-catalyst supramolecular assembly via axial coordination of a cobalt-based H_2-evolving catalyst, *i.e.* a cobaloxime complex, to a pyridyl-functionalized Ru-diacetylide photosensitizer. The new supramolecular assembly was employed for the construction of NiO-based photocathodes and subsequent H_2 generation under pertinent aqueous conditions (Figure 1).
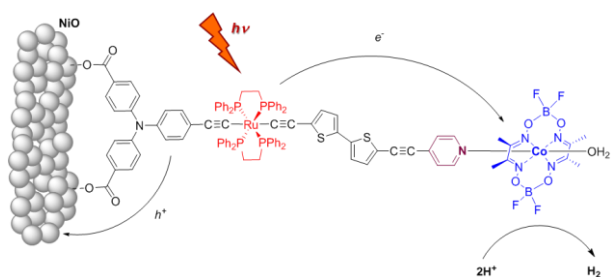

Figure 1. Representation of the **Ru-diacetylide/Cobaloxime** assembly anchored onto a mesoporous NiO (nanoparticulate) thin-film.

RESULTS AND DISCUSSION

Synthesis and characterization.

The synthetic route to the new multicomponent system and the relevant precursors are depicted in Scheme 1. Synthesis of the alkynyl ligand bearing the pyridine coordinating group was achieved in three steps involving successive Sonogashira coupling reactions and subsequent deprotection of the alkyne function to give **3**. Then, according to established procedure for the synthesis of asymmetric diacetylide complexes featuring the $\{Ru(dppe)_2\}^{2+}$ metal center,[41] the activation of the terminal alkyne of **3** by the ruthenium-vinylidene moiety **4**, described earlier,[39] in the presence of a non-coordinating salt ($NaPF_6$) and a base (Et_3N), afforded the dialkynyl intermediate **5**. The carboxylic acid anchoring functions of **4** were protected with silyl-ester groups, i. e. 2-(trimethylsilyl)ethyl (TMSE), in order to avoid side reactions with the metal centre during the different organometallic synthesis steps. Subsequent deprotection of the silyl-ester groups under mild conditions, using tetrabutyl ammonium fluoride in THF at room temperature, afforded the target photosensitizer **6** in good yields. Finally, the reaction of **6** with the $[Co(dmgBF_2)_2(OH_2)_2]$ (dmg = dimethylglyoxime) cobaloxime **7**, afforded the supramolecular photocatalytic system **6-Co**.

The Ru-based complexes **5** and **6** were characterized by means of ^{31}P, ^1H and ^{13}C NMR, FT-IR spectroscopies and HR-MS. The *trans*-ditopic structure of the metal centre was confirmed by the ^{31}P NMR spectrum which shows a singlet for the four equivalent phosphorus atoms, with $\delta \approx 53$ ppm characteristic of the Ru-diacetylide structure.[41-43] Characteristic peaks were observed on the infra-red spectra, at *ca.* 2195 cm^{-1} for the $\nu_{C\equiv C}$ of the ethynylpyridine unit and at *ca.* 2040 cm^{-1} corresponding to the $\nu_{C\equiv C}$ stretching vibration of the metal-alkynyl ligands.

Good quality NMR analysis of **6-Co** was impeded by the presence of the paramagnetic Co^{II} metal centre. Nonetheless, the infra-red spectrum of **6-Co** confirmed the preservation of the photosensitizer's structure as characteristics peaks of the $\nu_{C\equiv C}$ stretching vibrations remained

unchanged. Additional peaks corresponding to the cobaloxime moiety were observed at 1611 cm^{-1} ($\nu_{C=N}$), 1012 cm^{-1} (ν_{N-O}) and 825 cm^{-1} (ν_{B-O}). Furthermore, evidence for the formation of a coordination complex between **6** and the cobaloxime moiety was afforded by ESI+ HR-MS spectrometry (see Figure S1) which shows a peak at 1959.50152 corresponding to de-hydrated complex **6-Co** – H$_2$O (M – H$_2$O)$^+$ and by electrochemistry (see below).

Scheme 1. Synthesis route to **[Ru-Co]** supramolecular assembly.[i]
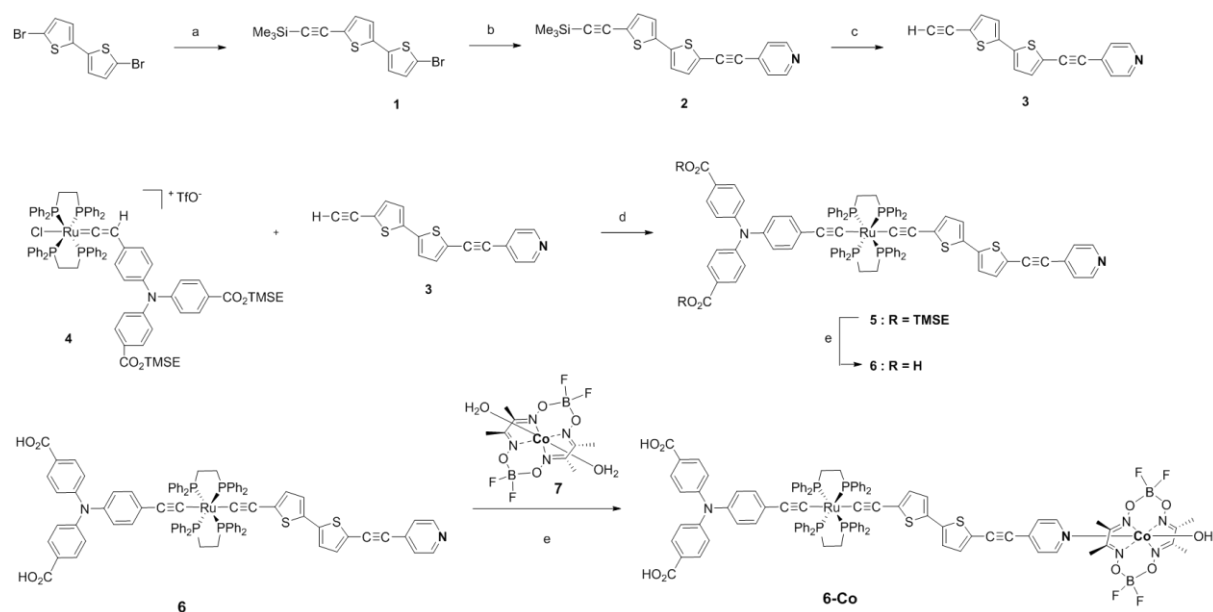
[i]Conditions: (a) Trimethylsilylacetylene, PdCl$_2$(PPh$_3$)$_2$, CuI, diisopropylamine, THF; (b) 4-ethynylpyridine hydrochloride, PdCl$_2$(PPh$_3$)$_2$, CuI, diisopropylamine, THF; (c) K$_2$CO$_3$, MeOH ; (d) NaPF$_6$, Et$_3$N, CH$_2$Cl$_2$; (e) TBAF, THF; (f) THF.

Optical and electrochemical properties.

UV-visible absorption spectra of the photocatalytic system **6-Co** and of the parent photosensitizer **6**, recorded in THF solution, are presented in Figure 2 and the corresponding data are gathered in Table 1. In these spectra, intense absorption bands are observed in the UV region, below 300 nm, characteristic of the phenyl substituents of the diphosphine ligands.[42] According to previous reports, the intense absorption band centered at *ca.* 355 nm can be attributed to electronic transitions involving the electron-rich triphenylamine ligand.[39] A broad absorption band is observed in the visible region with maximum wavelength at 463 nm and ε ≈ 12 000 M^{-1}.cm^{-1}, corresponding to multiple metal-to-ligand charge transfer (MLCT) transitions

6

involving the $\{Ru(dppe)_2\}^{2+}$ metal center. Interestingly, the formation of the photocatalytic system through pyridyl-coordination of the cobaloxime moiety to the Ru complex **6** does not affect the absorption properties of the photosensitizer. The weak contribution of **7** in the electronic absorption spectrum of **6-Co** is not discernable from the absorption of the dye and no significant electronic transition seems to occur between the $\{Ru(dppe)_2\}^{2+}$ metal center and the cobaloxime moiety. The zero-zero transition energy was estimated from the onset of the absorption spectra, leading to $E_{0-0} = 2.25$ eV for both **6** and **6-Co**.
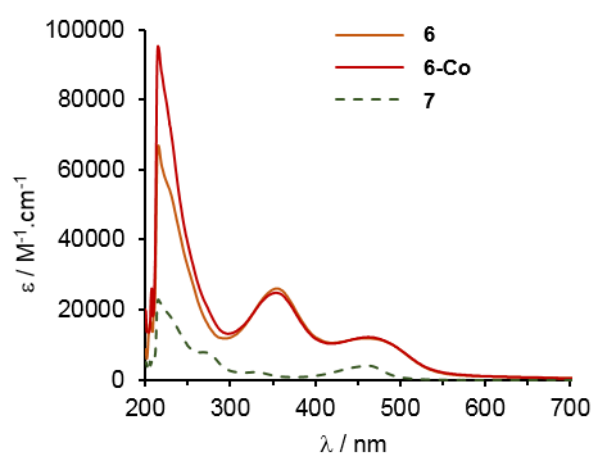

Figure 2. Absorption spectra of **6**, **6-Co** and **7** in THF (C ~ 1.10^{-5} M).

Table 1. Optical and electrochemical properties.

	λ_{max} [nm]	ε [$M^{-1}.cm^{-1}$]	E_{0-0} [eV][a]	E_{red2} [V vs. Fc^+/Fc][b]	E_{red1} [V vs. Fc^+/Fc][b]	E_{ox} [V vs. Fc^+/Fc][b]	E_{red2} [V vs. NHE][d]	E_{red1} [V vs. NHE][d]	E_{ox} [V vs. NHE][d]	$E^{-/*}$ [V vs. NHE][e]
6	463 356	11 900 26 000	2.25	-	-	+ 0.02 (100)[c]	-	-	+ 0.75	-
6-Co	463 355	12 200 24 800	2.25	− 2.20 (120)[c]	− 1.05 (120)[c]	-0.02 (90)[c]	− 1.47	− 0.32	+ 0.71	+ 0.78
7	462 270	4 000 7 900	-	-	− 1.12 (105)[c]	-	-	− 0.39	-	-

Absorption spectra in THF. [a] 0-0 transition energy estimated from the onset of the absorption spectra. [b] Redox potentials in DMF solution. [c] $\Delta E p_a$-$E p_c$ [mV]. [d] Redox potentials referred to NHE by addition of 730 mV.[44] [e] Reduction potential of the excited state obtained from E_{red2}+E_{0-0}

The electrochemical properties of **6-Co** and the parent compounds **6** and **7** were investigated by cyclic voltammetry in DMF solution (Figure S2), the corresponding data are reported in Table 1. The Ru-diacetylide complex **6** shows two reversible mono-electronic processes in the anodic region, that can be attributed to the oxidation of the electron-rich π-conjugated system of the dye, including the $\{Ru(dppe)_2\}^{2+}$ fragment. The first oxidation process occurs at $+ 0.02$ V *vs.* Fc^+/Fc. The cobaloxime **7** shows as well-defined reversible monoelectronic wave in the cathodic region, located at $- 1.12$ V *vs.* Fc^+/Fc and corresponding to the $Co^{II} \rightarrow Co^{I}$ reduction process. As expected, the voltammogram of **6-Co** displays both contributions of the Ru-based photosensitizer and of the cobalt catalyst. In the anodic part, the two oxidation waves are conserved, however the first oxidation potential of **6-Co** is shifted by 40 mV toward more negative potentials upon coordination of the dye to the cobaloxime moiety ($E_{ox\ \textbf{6-Co}} = - 0.02$ V *vs.* Fc^+/Fc). Conversely, in the cathodic part, the reduction process involving the Co core is shifted to more positive values by 70 mV, $E_{red\ \textbf{6-Co}} = - 1.05$ *vs.* Fc^+/Fc . This positive shift of the reduction potential of a cobaloxime moiety is characteristic of the coordination by a pyridyl ligand.[6, 7] Besides, this feature provides good evidence for the formation of the supramolecular photocatalytic system **6-Co**. In addition a second reduction process is now visible at more cathodic potential ($E_{red2\ \textbf{6-Co}} = - 2.20$ V *vs.* Fc^+/Fc). From these data, we could determine the redox properties of the excited state of **6-Co** (Table 1) and construct the energy diagram of a NiO-based photocathode designed for H_2-evolution in water and sensitized by **6-Co**, as shown in Figure 3. After initial light excitation, very fast hole injection from the dye excited state to the NiO valence band is expected to occur; this process was indeed reported to take place on sub-ps to a few tens of picosecond timescales for related NiO-based dye-sensitized photocathodes.[38,45,46] This will generate at the surface of the film the reduced dye, which is then able to reduce the catalytic center by thermal electron transfer. The latter is active for the reduction of protons in H_2 through a mechanism that involves protonation of the Co^{I} state of

the catalyst to generate a Co^{III}-H intermediate (**6-CoH**) and subsequent light-driven reduction of this intermediate to a Co^{II}-H species, the protonation of which yields H_2 and regenerates the initial Co^{II} center.
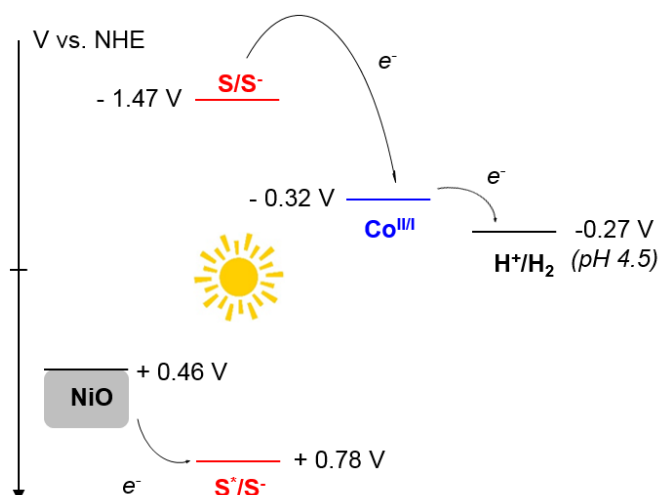

Figure 3. Energy diagram of a NiO-based photocathode including **6-Co** (S stands for the sensitizing part of the photocatalytic system, *i.e.* the Ru-based dye).

Theoretical calculations.

Quantum chemical calculations were performed to gain deeper insight into the electron-density distribution of the frontier molecular orbitals and to assess the electronic transitions occurring upon photoexcitation of the sensitizer **6** and of the photocatalytic system **6-Co**.

The calculated ground-state minimum-energy molecular structures of **6** and **6-Co** are shown in Figure S3, spatial representations of the corresponding HOMO (Highest Occupied Molecular Orbital) and LUMO (Lowest Unoccupied Molecular Orbital) are represented in Figure 4.

The calculations show that in **6** the HOMO is spread over the whole π-conjugated system of the dye, including the $\{Ru(dppe)_2\}^{2+}$ core and the two acetylide ligands. However, significant electron-density is observed on the triphenylamine unit as well as on the two anchoring groups, which would favor electron transfers from NiO to the grafted dye.[47] On the other hand, the LUMO of the dye is localized on the electron-poor ligand bearing the pyridine ring. Good charge separation therefore occurs within this Ru-diacetylide complex. The HOMO in **6-Co**

retains the same feature as in **6**, the electron density being spread over the whole π-conjugated system, but no density is observed on the cobaloxime moiety and thus, the electronic conjugation ends up at the pyridine ring. Interestingly, the LUMO in **6-Co** owns electron-density on the Co atom, and thus the electron transfer from the sensitizer to the catalyst can be barrierless in the excited state. As a consequence, the calculations highlight the appropriate electronic density distribution of the frontier molecular orbitals in **6-Co**, favorable to the electron transfer processes occurring within a DS-PEC.
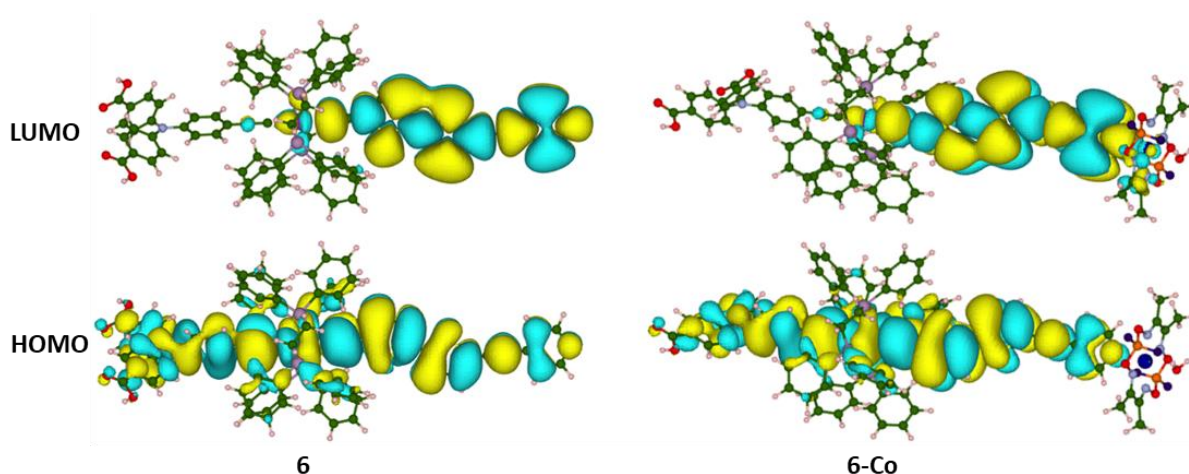
Figure 4. Isodensity surface plots of the HOMO and LUMO of **6** and **6-Co** (contour value set to 0.005 a.u.). Color legend: C atom green, O atom red, N atom light blue, Ru atom magenta, H atom white, S atom yellow, P light purple; isodensity positive and negative values are depicted in yellow and cyan, respectively.

The binding energy relative to the formation of **6-Co** according to equation (1) was investigated through theoretical calculations.

$$\textbf{6} + \textbf{7} \rightarrow \textbf{6-Co} + \textbf{H}_2\textbf{O} \qquad \text{equation (1)}$$

The calculated enthalpy of the reaction is $\Delta H = -1.14$ eV (-110.0 kJ/mol) and the calculated Gibbs free-energy of the formation of the system is $\Delta G = -0.14$ eV (-13.5 kJ/mol). Both values indicate that the formation of **6-Co** through pyridyl-coordination of the cobaloxime **7** is strongly favored.

Table 2. TD-DFT calculated electronic properties (CAM-B3LYP/SDD/6-31G(d)/PCM=THF/H_2O).

	ΔE_{calc} /eV [a]	λ_{calc} / nm [b]	f [c]	Electronic transition assignment [d]
6 (THF)	2.79 3.74	445 332	2.023 0.589	HOMO → LUMO (72%) HOMO-1 → LUMO+1 (37%)
6 (H_2O)	2.80 3.74	443 331	2.013 0.576	HOMO → LUMO (71%) HOMO-1 → LUMO+1 (36%)
6-Co (H_2O)	2.73 3.76	455 330	2.180 0.584	HOMO → LUMO (68%) HOMO-1 → LUMO+3 (35%)
6-CoH (H_2O)	2.67 3.76	465 330	2.235 0.585	HOMO → LUMO (66%) HOMO → LUMO+4 (37%)

[a] ΔE_{calc} = main transition energy. [b] λ_{calc} = calculated λ_{max}. [c] f = oscillator strength. [d] Main Kohn-Sham orbital contribution to the electronic transition.

The electronic structure corresponding to the minimum energy structures of the dye (**6**) and the dye-catalyst complex (**6-Co**) were further characterized by means of TD-DFT calculations. The parameters relative to the main photoinduced electronic transitions are given in Table 2. The two main transition energies calculated for **6** in THF are in good accordance with the experiment, the small deviation being attributable to the large size of the complex and to known limitations of TD-DFT for charge-transfer excitation.[48] The transition assignment reveals that the lowest-energy transition, corresponding to λ_{calc} = 445 nm, owns a major HOMO → LUMO character, while the higher-energy transition, corresponding to λ_{calc} = 332 nm, presents a HOMO-1 → LUMO+1 character. The calculations give very similar results when carried out with H_2O as the implicit solvent. The main transition energies calculated for **6-Co** in H_2O also match the experiment, the lowest-energy transition being predicted at λ_{calc} = 455 nm.

Considering the hydrogen evolution reaction (HER) mechanism,[11, 15] the first addition of a proton and an electron to the **6-Co** complex leads to the formation of a Co-H bond where the Co is in a 3^+ state (low spin d^6, singlet) and the hydrogen has an hydride nature. We characterized such complex **6-CoH** in water with the same theoretical scheme. The stability of this intermediate was computed considering the reaction:

$$\textbf{6-CoH} \rightarrow \textbf{6} + \textbf{CoH} \qquad \text{equation (2)}$$

The calculated enthalpy of the reaction (eq. 2) is $\Delta H = 0.827$ eV (79.8 kJ/mol) and the corresponding Gibbs free-energy is $\Delta G = 0.221$ eV (21.3 kJ/mol). In this case, the positive values of both ΔH and ΔG indicate that upon formation of the Co(III)-H intermediate, the dissociation of the dye-catalyst complex is not favored and its stability is retained.

The structural changes going from 6-Co to 6-CoH involve mainly the Co center, the distance between the 6 pyridine N atom and the cobalt goes from 2.310 Å in 6-Co to 2.108 Å in 6-CoH, as well the average distance between Co and the cobaloxime N atoms goes from 1.905 Å in 6-Co to 1.892 Å in 6-CoH. These results are consistent with the shift from the Co(II) in 6-Co to the Co(III)-H$^-$ specie in 6-CoH.

TD-DFT calculation were also pursued on such **6-CoH**, the reaction intermediate for hydrogen evolution reaction (HER).[11, 15] Interestingly the formation of the HER intermediate **6-CoH** does not affect the optical properties of the photocatalytic system. The two main transition energies are conserved with $\lambda_{calc} = 445$ nm and 330 nm, as well as the nature of the frontier orbitals involved in the lowest-energy transition which presents a major HOMO → LUMO character. These theoretical results highlight two key points for photocatalysis: the thermodynamic stability and the light absorbing properties of the dye-catalyst complex before each of the two H^+/e^- transfer steps of the HER mechanism.

Electrode preparation and characterization – XPS analyses

The photocatalytic system **6-Co** was then used to prepare a photocathode for H_2 evolution based on F108-templated mesoporous NiO films.[37] Sensitization was achieved by soaking the semiconducting porous layer in a DMF solution of **6-Co** (0.5 mM) for 24 h at RT. The absorption spectrum of the sensitized electrode is depicted in Figure S5. An increase of absorption is observed in the 350-500 nm wavelength region as expected. The amount of dye-loading on the photoelectrode was quantified by dye desorption under mild conditions using a phenylphosphonic acid solution (1 M in DMF).[49] The estimated quantity of dye on the 1-μm thick NiO film was estimated to be about 6.2 nmol.cm^{-2}, which is in the same range as those determined in previous studies using similar electrodes.[39, 40]

The presence of Ru and Co atoms at the surface of NiO electrodes sensitized with either **6** or **6-Co** was further investigated through X-ray photoelectron spectroscopy (XPS) analyses. The study was extended to pristine powders of **6**, **7** and **6-Co** for comparison (Figure S6). The survey spectrum of pristine **6-Co** shows peaks of Ru3p3, Co2p, C1s, O1s, N1s, S2p and S2s, P2p and P2s, F1s and B1s. This spectrum is fully consistent with the XPS surveys of **6** and **7,** and confirms the presence of expected chemical elements for **6-Co**. After chemisorption of **6-Co** onto NiO, the survey spectrum of the resulting material **6-Co@NiO** (Figure S7) shows the same features, along with those of NiO *i.e.* peaks attributed to Ni2p photoelectrons and NiLMM Auger, but also additional information such as an increase of C, presence of N, S and P. High-resolution core level spectra were recorded to further characterize the electrodes. The presence of the Ru metallic centers in **6@NiO** and **6-Co@NiO** is mainly confirmed by the signals of Ru3d$_{5/2}$ level in the 280-282 eV region, which is characteristic of Ru(II) species.[50, 51]. Fitted C1s-Ru3d$_{3/2}$-Ru3d$_{5/2}$ spectra of **6-Co@NiO** are shown in Figure 5a.
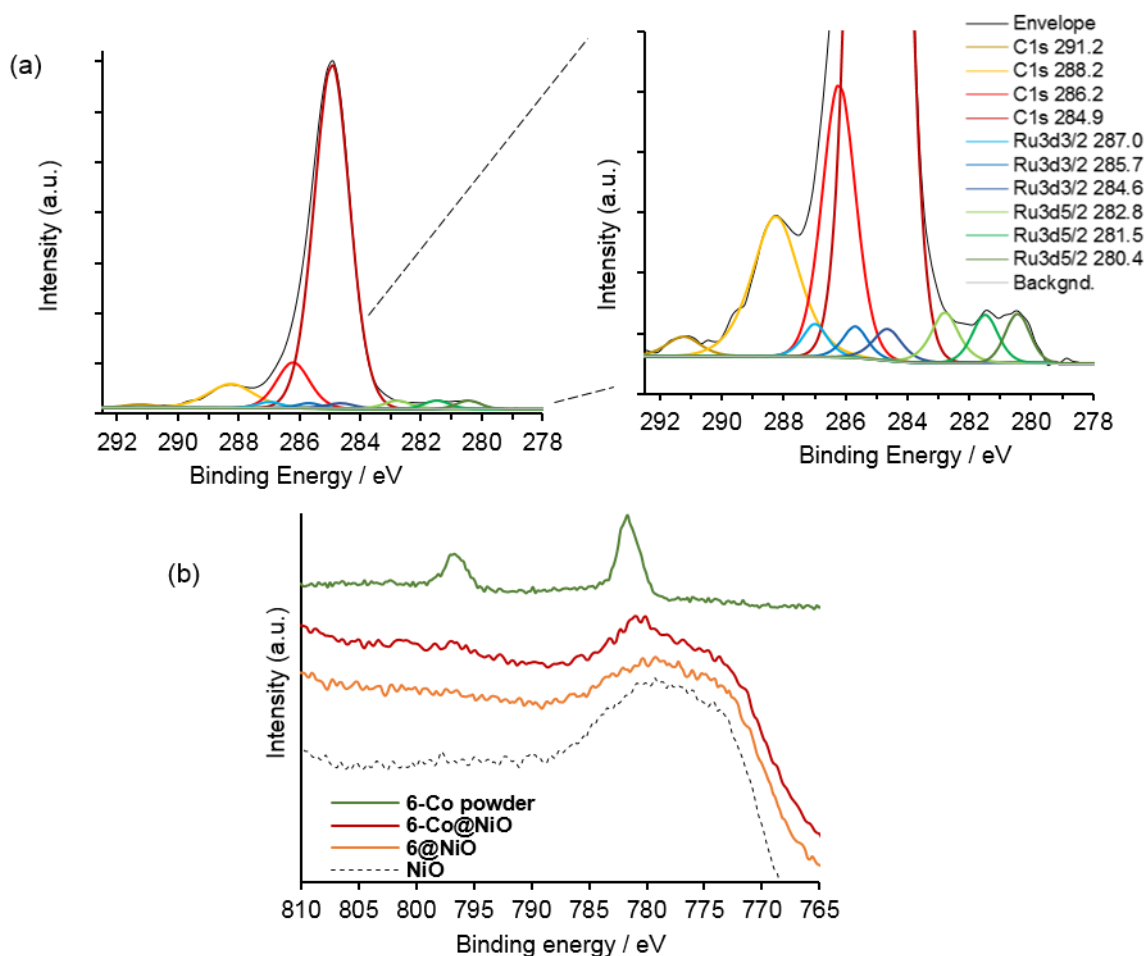
Figure 5. XPS core level spectra of **6-Co**@NiO in the Ru_{3d}–C_{1s} (a) and Co_{2p} (b) core regions.

Finally, a broad band at 770-780 eV corresponding to Ni *LMM* Auger was detected in the 765-810 eV region for bare NiO and **6@NiO** (Figure 5b). By contrast, new features at 780 eV and 796 eV, typical of Co 2p3/2 and Co 2p1/2 levels, along with the broad band at 770-780 eV were observed for **6-Co@NiO**. These results are fully consistent with the presence of Co(II) metal centers at the surface of the NiO electrode sensitized by **6-Co**.[31, 37]

As a consequence, XPS data clearly evidence the successful chemisorption of **6-Co** onto NiO electrodes.

Photoelectrochemical properties

The photoelectrochemical properties of the **6-Co@NiO** photocathode were finally evaluated in aqueous solution (acetate buffer, pH 4.5). Linear sweep voltammograms were recorded in the dark and under visible-light irradiation (Figure S8). As expected a cathodic photocurrent is

observed under light with a density of *c.a.* 5.6 µA. cm^{-2} at + 0.07 V *vs.* RHE (− 0.4 V *vs.* Ag/AgCl). This behavior is due to photoinduced electron transfers from the p-type semi-conductor NiO, to the cobaloxime catalyst, through excitation of the sensitizer part in **6-Co**. Chronoamperometric measurements were performed under chopped-light at different applied potentials (+ 0.47 V, + 0.27 V, + 0.07 V *vs.* RHE) over a period of 10 minutes showing steady-state cathodic photocurrent generation (Figure S9). The maximum magnitude was obtained at the most cathodic potential, *i.e.* + 0.07 V *vs.* RHE (− 0.4 V *vs.* Ag/AgCl), with a photocurrent density of *ca.* 3.2 µA. cm^{-2} (Figure 6). Interestingly, the traces recorded for the electrodes sensitized with **6-Co** display cathodic photocurrent spikes when light is switched on (Figures 6 and S9), which is not observed in the absence of catalyst (**6**-sensitized film, orange trace in Figure 6). These spikes are attributed to a relatively slow proton reduction kinetics at the cobalt center, leading to charge accumulation at the electrode/electrolyte interface before reaching an equilibrium state, in which catalytic H$_2$ production consumes photogenerated charges. This is confirmed by the absence of any reverse anodic spike (Figure 6), when light is switched off. Actually, at the most positive potential (+0.47 V vs RHE in Figure S9), catalysis is slower (lower photocurrent density) and the cathodic spikes are much more intense. This results in a higher amount of accumulated charges which cannot all be consumed by catalytic H$_2$ evolution, as evidenced by the presence of small anodic spikes when light is switched off. A similar behaviour was previously observed for a related cobaloxime-based photocathode.[36]
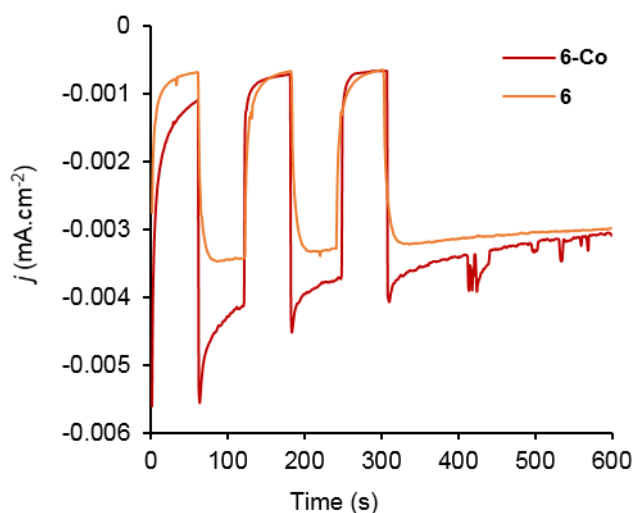
Figure 6. Chronoamperometric measurements under chopped-light using NiO electrodes sensitized with **6-Co** (red line) or **6** only (orange line) in acetate buffer (0.1 M, pH 4.5) at an applied potential of + 0.07 V vs. RHE (– 0.4 V vs. Ag/AgCl) under visible-light irradiation (400-800 nm, 65 mV.cm^{-2}, 1 sun).

Thus, photoelectrochemical H$_2$ evolution was investigated by long-term electrolysis (Figure S10) at an applied potential of + 0.07 V *vs.* RHE (– 0.4 V *vs.* Ag/AgCl) in acetate buffer (0.1 M, pH 4.5) under visible-light irradiation (400-800 nm, 65 mW.cm^{-2}, equivalent to 1 sun irradiation). The cathodic charge passed through the photoelectrode during the course of the electrolysis was Q = 78 mC over a period of 4h30. Gas chromatographic analysis of the headspace confirmed the photo-electrochemical generation of H$_2$ with a faradaic yield of 27 %. This yield is relatively low but is in the range of state-of-the-art NiO-based dye-sensitized H$_2$-evolving photocathodes.[30] Competing reactions, such as the NiO reduction,[37,52] or reduction of the oxygen formed in the anodic compartment (which might diffuse during the course of long-term experiments), might be considered. A slow decrease of the photocurrent (from 2.5 to 1 µA.cm^{-2}) is also observed during the course of the 4.5 hours measurement, which can be attributed – at least partly – to some leaching of the dye-catalyst assembly in the electrolyte. Control experiment using a NiO-electrode sensitized with **6** only confirmed steady-state photocurrent generation however with a slightly lower magnitude, *ca.* 2.2 µA. cm^{-2} at + 0.07 V *vs.* RHE (Figure 6). The absence of cathodic spikes (orange trace in Figure 6) underlines that

16

the recorded photocurrent corresponds to a distinct and competitive faradaic process. Long-term electrolysis over a period of 5h30 indeed led to a cathodic charge of $Q = 144$ mC however with almost no H_2 detected in the headspace (0.3% FY). This small amount of H_2 may be catalyzed by in situ light-driven formation of Ni nanoparticles, as previously described[52] and also observed by XPS in a similar system.[37] This experiment confirms that the photocatalytic system **6-Co** is the active species for H_2 evolution in our NiO-based DS-PEC.

The observation of catalytic H_2 evolution with NiO-grafted **6-Co** confirms previous reports on photoelectrochemical systems containing a pyridine-coordinated cobaloxime catalyst[27, 28, 36] and indicates that the cobaloxime moiety remains bound to the photosensitizer despite a potentially weak Co-N(pyridine) coordination linkage. In particular, work by Wasielewski *et al.*[53] demonstrated fast dissociation of the reduced cobaloxime moiety from photosensitizer upon excitation in a pyridyl-xylene-1,8-naphthalimide-cobaloxime assembly. However, recent work from our group allowed to conclude that pyridine ligand likely remains coordinated to Co(I) at least at the timescale of cyclic voltammetry.[54] Furthermore, DFT calculations reveal that protonation of the Co(I) intermediate forms a Co(III)-H species with strong affinity with pyridine ligands and support catalytic H_2 evolution at the surface of the dye-sensitized NiO photoelectrode.

17

CONCLUSION

This study demonstrates that dyes with an original π-conjugated structure including the [Ru(dppe)$_2$] metal fragment with σ-alkynyl ligands bearing donor and acceptor groups, *i.e.* a triphenylamine donor unit and a thiophene-ethylnylpyridine acceptor group are suitable for the construction of efficient photoelectrodes for H$_2$ evolution from water after grafting onto NiO substrates and combination with cobaloximes through Co-coordination of their pyridine function. The photoelectrochemical performances proved similar to previously reported molecular photocathodes at neutral pH in phosphate buffer, showing that this family of sensitizers can rival with the prototypical ruthenium tris-diimine dyes in that context,[27, 28, 36] while providing more versatility in terms of synthesis and combination of various donor and acceptor functions. Further work will target the optimization of the light-harvesting properties of such chromophores as well as their combination with novel p-type transparent materials such as delafossites CuGaO$_2$[55] and CuCrO$_2$,[30] which already proved promising in this context.

EXPERIMENTAL SECTION

Materials and methods. The reactions were carried out under inert atmosphere using the Schlenk techniques. Solvents were dried from appropriate drying agents (sodium for pentane, diethyl ether and THF; calcium hydride for dichloromethane, chloroform and methanol) and freshly distilled under nitrogen before use. All reagents were obtained from commercially available sources and used without further purification. Compounds **4** and **7** were synthesized according to reported procedures. [39, 56]

^{1}H NMR, ^{13}C NMR and ^{31}P NMR analyses were performed on Bruker Avance I 300 MHz, Avance II 400 MHz and Avance III 600 MHz spectrometers. Chemical shift values are given in ppm with reference to solvent residual signals.[57] HR-MS analyses were performed by the CESAMO and IECB platform (Bordeaux, France). Field desorption (FD) measurements were carried out on a TOF mass spectrometer AccuTOF GCv using an FD emitter with an emitter voltage of 10 kV. One to two microliters solution of the compound were deposited on a 13µm emitter wire. FT-IR spectra were recorded on a Perkin Elmer Spectrum 100 spectrometer using KBr pellets. UV-visible absorption spectra were recorded on a UV-1650PC SHIMADZU spectrophotometer.

Cyclic voltammetry analyses were performed using a potentiostat/galvanostat Autolab PGSTAT100 and a three-electrode system (working electrode: Pt disc; reference electrode: Ag/AgCl, calibrated with ferrocene as internal reference; counter electrode: Pt) with 0.1M Bu$_4$NPF$_6$ as salt support at a scan rate of 100 mV.s^{-1}.

XPS surface analysis were realised using a ThermoFisher Scientific K-ALPHA spectrometer with a monochromatized AlKα source (hν=1486.6eV) and a 400 microns X-Ray spot size. A pressure of 10^{-7} Pa was applied in the chamber when transferring the samples coated onto indium foil for the powders or maintained by aluminium tape for the electrodes. The full survey spectra (0-1100 eV) were obtained with a constant pass energy of 200eV and high resolution

spectra at a constant pass energy of 40eV. Charge neutralization was applied during analysis. High resolution spectra (i.e. C1s-Ru3d, O1s, N1s, B1s, F1s, S2p, P2p, Ni2p, Co2p) were quantified and/or fitted using the AVANTAGE software provided by ThermoFisher Scientific (Scofield sensitivity factors used for quantification).

Synthesis of 1. 5,5'-Dibromo-2,2'-bithiophene (1.00 g, 3.09 mmol, 1 eq.), $PdCl_2(PPh_3)_2$ (108.3 mg, 0.15 mmol, 5%) and copper(I) iodide (14.7 mg, 0.077 mmol, 2.5%) were introduced in a Schlenk flask under nitrogen and dissolved in a mixture of diisopropylamine (20 mL) and dry THF (20 mL). Ethynyltrimethylsilane (TMSA) (0.39 mL, 2.8 mmol, 0.9 eq.) was subsequently added into the Schlenk flask. The suspension was stirred at RT for 1 h. Then the reaction mixture was poured into pure water and the solution was extracted with hexane. The crude product was evaporated to dryness and purified on silica gel column (hexane) to give **1** as an earth yellow powder in 50 % yield (0.48 g, 1.41 mmol). ^{1}H NMR (300 MHz, CD_2Cl_2): δ = 7.12 (d, 1H, $^3J_{HH}$ = 3.83 Hz), 7.00 (d, 1H, $^3J_{HH}$ = 3.89 Hz), 6.98 (d, 1H, $^3J_{HH}$ = 3.83 Hz), 6.95 (d, 1H, $^3J_{HH}$ = 3.89 Hz), 0.25 (s, 9H). ^{13}C NMR (75 MHz, CD_2Cl_2): δ = 138.45, 138.03, 133.86, 131.33, 124.90, 124.09, 122.71, 112.06, 100.86, 97.23, 0.15.

Synthesis of 2. Compound **1** (0.758 g, 2.22 mmol, 1 eq.), 4-ethynylpyridine hydrochloride (0.3719 g, 2.66 mmol, 1.2 eq.), $PdCl_2(PPh_3)_2$ (77.9 mg, 0.11 mmol, 5%) and copper(I) iodide (10.6 mg, 0.056 mmol, 2.5%) were introduced in a Schlenk flask under nitrogen and dissolved in a mixture of diisopropylamine (15 mL) and dry THF (15 mL). The solution was stirred at RT for 24 h. After evaporation of the solvent, the mixture was dissolved with ethyl acetate and washed with water. The resulting crude product was evaporated to dryness and purified on silica gel column (ethyl acetate/pentane (8:2, v/v)) to give **2** as a yellow powder in 79 % yield (0.636 g, 1.75 mmol). ^{1}H NMR (300 MHz, CD_2Cl_2): δ = 8.59 (s, 2H), 7.37 (d, 2H, $^3J_{HH}$ = 5.80 Hz),

7.28 (d, 1H, $^3J_{HH}$ = 3.88 Hz), 7.15 (d, 1H, $^3J_{HH}$ = 3.86 Hz), 7.13 (d, 1H, $^3J_{HH}$ = 3.88 Hz), 7.09 (d, 1H, $^3J_{HH}$ = 3.85 Hz), 0.25 (s, 9H). ^{13}C NMR (75 MHz, CD$_2$Cl$_2$): δ = 150.22, 139.77, 137.99, 134.76, 133.98, 131.04, 125.39, 124.74, 123.34, 121.57, 114.17, 101.27, 97.19, 92.18, 87.11, 0.16.

Synthesis of 3. Compound **2** (0.513 g, 1.41 mmol, 1 equiv.) and potassium carbonate (0.019 g, 0.14 mmol, 0.1 eq.) were dissolved in distilled methanol (25 mL) under nitrogen. The mixture was stirred at RT for 24 h before being poured into water. The organic phase was recovered with ethyl acetate and evaporated to dryness. The crude product was purified by chromatography on silica gel (ethyl acetate/pentane (8:2, v/v)) to afford **3** as an orange powder in 72 % yield (0.2976 g, 1.02 mmol). ^{1}H NMR (300 MHz, CD$_2$Cl$_2$): δ = 8.60 (m, 2H), 7.37 (m, 2H), 7.29 (d, 1H, $^3J_{HH}$ = 3.83 Hz), 7.21 (d, 1H, $^3J_{HH}$ = 3.82 Hz), 7.14 (d, 1H, $^3J_{HH}$ = 3.91 Hz), 7.11 (d, 1H, $^3J_{HH}$ = 3.87 Hz), 3.51 (s, 1H). ^{13}C NMR (75 MHz, THF-d$_8$): δ = 150.72, 139.83, 138.21, 135.19, 134.64, 130.86, 125.35, 125.18, 122.88, 121.88, 117.80, 92.49, 86.76, 84.76, 76.78.

Synthesis of 5. Compounds **4** (0.500 g, 0.31 mmol, 1 eq.), **3** (0.106 g, 0.37 mmol, 1.2 eq.) and NaPF$_6$ (0.102 g, 0.61 mmol, 2 eq.) were dissolved in dry CH$_2$Cl$_2$ under nitrogen atmosphere. Et$_3$N (0.17 mL, 1.22 mmol, 4 equiv.) was subsequently added and the suspension was stirred at RT for 36 h. The reaction mixture was then diluted with CH$_2$Cl$_2$ and washed with pure water. The organic phase was evaporated to dryness. The resulting solid was washed with pentane and dried under reduced pressure to afford **5** as a red powder in 74 % yield (0.393 g, 0.23 mmol). 31P NMR (120 MHz, CD$_2$Cl$_2$): δ = 52.5. ^{1}H NMR (300 MHz, CD$_2$Cl$_2$): δ = 8.59 (m, 2H), 8.00-6.79 (m, 56H), 4.39 (m, 2H), 2.51 (m, 8H), 1.12 (m, 2H), 0.08 (s, 9H). ^{13}C NMR (200 MHz, THF-d$_8$): δ = 204.17, 195.29, 166.97, 165.93, 150.69, 135.17, 134.69, 131.93, 131.84, 131.69, 131.57, 131.35, 129.48, 129.26, 127.80, 126.66, 126.42, 125.21, 124.96, 122.81, 122.39, 118.82, 117.92, 110.00,

91.81, 87.80, 67.78, 63.15, 62.85, 54.62, 31.99, 30.16, 17.94, 1.12, -1.62. HR-MS FD$^+$ (m/z): 1744.4719 [M]$^+$ (calcd. 1744.4213 for [C$_{101}$H$_{94}$N$_2$O$_4$P$_4$RuS$_2$Si$_2$]$^+$). FT-IR (KBr): $\nu_{C\equiv C}$ = 2196 cm^{-1}, $\nu_{C\equiv C}$ = 2040 cm^{-1}, $\nu_{C=O}$ = 1709 cm^{-1}, ν_{P-Ph} = 1099 cm^{-1}, ν_{Si-C} = 836 cm^{-1}.

Synthesis of 6. To a solution of **5** (470 mg, 0.27 mmol, 1 eq.) in dry THF (50 mL) and under inert atmosphere was added TBAF (1M sol. in THF, 1.08 mL, 1.08 mmol, 4 eq.). The reaction mixture was stirred at RT for 24 h. After removal of the solvent the resulting solid was dissolved in CH$_2$Cl$_2$ and thoroughly washed with degassed citric acid aqueous solution (10 % m) and then pure water. The organics were evaporated to dryness to afford **6** as a dark red powder in 69 % yield (0.288 g, 0.19 mmol). ^{31}P NMR (120 MHz, CD$_2$Cl$_2$): δ = 52.9. ^{1}H NMR (300 MHz, THF-d$_8$): δ = 10.82 (s, 2H), 8.56 (m, 2H), 7.97-6.85 (m, 60H), 2.47 (m, 8H). ^{13}C NMR (100 MHz, THF-d$_8$): 166.21, 165.98, 151.02, 150.29, 150.02, 142.08, 141.11, 137.17, 136.76, 134.42, 133.92, 131.93, 132.35, 131.20, 131.11, 131.03, 130.85, 130.70, 129.74, 128.67, 128.47, 128.30, 127.86, 126.98, 126.34, 125.82, 125.56, 124.97, 124.64, 124.56, 124.42, 124.19, 123.73, 123.61, 123.50, 122.00, 121.57, 29.74. HR-MS FD$^+$ (m/z): 1544.2713 [M]$^+$ (calcd. 1544.2794 for [C$_{91}$H$_{70}$N$_2$O$_4$P$_4$RuS$_2$]$^+$). FT-IR (KBr): $\nu_{C\equiv C}$ = 2195 cm^{-1}, $\nu_{C\equiv C}$ = 2039 cm^{-1}, $\nu_{C=O}$ = 1709-1701 cm^{-1}, ν_{P-Ph} = 1099 cm^{-1}.

Synthesis of 6-Co. To a solution of **6** (30.8 mg, 0.02 mmol, 1 eq.) in dry THF (10 mL) and under inert atmosphere was added **7** (8.7 mg, 0.02 mmol, 1 eq.). The reaction mixture was stirred at RT for 4 h. After removal of the solvent, the resulting solid was further dried under vacuum to afford **6-Co** as a dark red powder in quantitative yield (39 mg). ^{31}P NMR (120 MHz, CD$_2$Cl$_2$): δ = 52.9. HR-MS ESI$^+$ (m/z): 1959.5015 [M-H$_2$O]$^+$ (calcd. 1959.3553 for [C$_{101}$H$_{88}$B$_2$CoF$_4$N$_6$O$_8$P$_4$RuS$_2$]$^+$). FT-IR (KBr): $\nu_{C\equiv C}$ = 2194 cm^{-1}, $\nu_{C\equiv C}$ =

2039 cm^{-1}, $\nu_{C\equiv O}$ = 1714-1684 cm^{-1}, $\nu_{C=N}$ = 1611 cm^{-1}, ν_{P-Ph} = 1098 cm^{-1}, ν_{N-O} = 1012 cm^{-1}, ν_{B-O} = 825 cm^{-1}.

Computational details.

The theoretical calculations were all carried out with the Gaussian09 quantum chemistry package.[58] All the ground state properties, i.e. minimum-energy structures, molecular frequencies and thermochemical data, were computed with the widely employed B3LYP hybrid density functional.[59] SDD effective core potentials for Ru and Co were employed together with the corresponding SDD basis sets.[60] For all the other atoms we employed the 6-31G(d,p) basis set.[61] Considering the large size of the system, this level of theory ensured the best compromise between accuracy and computational burden. The excited state properties have been computed with CAM-B3LYP long-range corrected hybrid density functional[62] that has been proven to be very effective for modeling vertical excitation with a Charge-Transfer character. In all the ground and excited states calculations we took into account the solvent medium (THF and water) by means of the Polarizable Continuum Model (PCM) of implicit solvation,[63] with the default parameters as implemented in Gaussian09.

Electrode preparation method.

F108-templated NiO films were spin coated onto FTO/glass substrates (Solems, TEC 7, sheet resistance 7Ω·□$^{-1}$) as previously reported.[25] NiO films sensitization was achieved by soaking the electrodes in DMF solutions of **6** or **6-Co** (0.5 mM) for 24 h at room temperature on an orbital stirring table. The electrodes were rinsed with DMF and CH$_3$CN, and dried in air.

Electrochemical and photoelectrochemical measurements.

Electrochemical and photoelectrochemical data were acquired with a Biologic VSP 300 potentiostat. Electrochemical measurements were conducted in a 3-electrode cell. The working electrode was a glassy carbon electrode in the reduction potential window and a Pt one in the oxidation potential window. The reference electrode was made of a Ag/AgCl wire dipped into

23

a KCl 3 M solution, separated from the supporting electrolyte by a Vycor® frit, and denoted below as Ag/AgCl. The counter electrode was a Pt wire. The supporting electrolyte was 0.1 M nBu_4NPF_6 in dry DMF. The supporting electrolyte was degassed with a flow of N_2 at least for 5 min before the measurements. The N_2 flow was removed from the solution but let in the headspace of the cell for the duration of the experiment. The concentration of the compound of interest was 1 mM. Cyclic voltammograms were typically recorded at a scan rate of 100 mV·s-1. The potential of the reference electrode was calibrated after each experiment by adding in the supporting electrolyte an internal reference (ferrocene for organic solvent, K_4FeCN_6 for aqueous solution), the potential of which was measured against the Ag/AgCl reference (0.43V for ferrocene and 0.24V for K_4FeCN_6).

Irradiation was carried out with a 300W ozone-free Xe lamp (Newport) operated at 280 W and mounted with a water-filled Spectra-Physics 6123NS liquid filter for elimination of IR ($\lambda > 800$ nm) irradiation and a Spectra-Physics 59472 UV cut-off filter ($\lambda < 400$ nm). The power density was calibrated using a Newport PM1918-R power-meter. The photocurrent measurements were carried out in a specifically designed three-electrode cell, using the NiO-sensitized film as the working electrode (3 to 3.5 cm^2), Ag/AgCl as the reference electrode and a Pt wire as the counter electrode. The counter electrode compartment was separated from the cathodic one by a Vycor® frit. The supporting electrolyte was a 0.1 M Sodium Acetate buffer at pH 4.5. The solution was degassed with nitrogen for 30 minutes prior to use. In a typical experiment, the volume of supporting electrolyte was 4.0 mL and the headspace was 2.4 mL. The photocathode was illuminated with a power density of 65 mW·cm^{-2} (ca. one sun). The amounts of evolved hydrogen were determined by sampling aliquots of the headspace in a Perkin Elmer Clarus 580 gas chromatograph equipped with a molecular sieve 5 Å column (30 m – 0.53 mm) and a TCD detector.

ASSOCIATED CONTENT

Supporting Information. Quantum chemical and XPS data. This material is available free of charge via the Internet at http://pubs.acs.org.

AUTHOR INFORMATION

Corresponding Authors

* E-mail: celine.olivier@u-bordeaux.fr, Tel: + 33 (0)5 4000 2425 (C. Olivier); E-mail: vincent.artero@cea.fr, Tel: + 33 (0)4 3878 9106 (V. Artero).

REFERENCES

[1]   Walter, M. G.; Warren, E. L.; McKone, J. R.; Boettcher, S. W.; Mi, Q.; Santori, E. A.; Lewis, N. S. Solar Water Splitting Cells. *Chem. Rev.* **2010**, *110*, 6446–6473.

[2]   Ardo, S.; Rivas, D. F.; Modestino, M. A.; Greiving, V. S.; Abdi, F. F.; Llado, E. A.; Artero, V.; Ayers, K.; Battaglia, C.; Becker, J. P.; Bederak, D.; Berger, A.; Buda, F.; Chinello, E.; Dam, B.; Di Palma, V.; Edvinsson, T.; Fujii, K.; Gardeniers, H.; Geerlings, H.; Hashemi, S. M. H.; Haussener, S.; Houle, F.; Huskens, J.; James, B. D.; Konrad, K.; Kudo, A.; Kunturu, P. P.; Lohse, D.; Mei, B.; Miller, E. L.; Moore, G. F.; Muller, J.; Orchard, K. L.; Rosser, T. E.; Saadi, F. H.; Schuttauf, J. W.; Seger, B.; Sheehan, S. W.; Smith, W. A.; Spurgeon, J.; Tang, M. H.; van de Krol, R.; Vesborg, P. C. K.; Westerik, P. Pathways to Electrochemical Solar-Hydrogen Technologies. *Energy Environ. Sci.* **2018**, 11, 2768-2783.

[3]   Gray, H. B. Powering the Planet with Solar Fuel, *Nature Chemistry*, **2009**, *1*, 7.

[4]   Gust, D.; Moore, T. A.; Moore, A. L. Solar Fuels via Artificial Photosynthesis. *Acc. Chem. Res.*, **2009**, *42*, 1890–1898.

[5]   Gasteiger, H. A.; Markovic, N. M. Just a Dream—or Future Reality? *Science*, **2009**, *324*, 48–49.

[6]   Fihri, A.; Artero, V.; Razavet, M.; Baffert, C.; Leibl, W.; Fontecave, M. Cobaloxime-Based Photocatalytic Devices for Hydrogen Production. *Angew. Chem. Int. Ed.*, **2008**, *47*, 564–567.

[7]   Fihri, A.; Artero, V.; Perreira, A.; Fontecave, M. Efficient H_2-producing Photocatalytic Systems Based on Cyclometalated Iridium- and Tricarbonylrhenium-diimine Photosensitizers and Cobaloxime Catalysts. *Dalton Trans.*, **2008**, 5567–5569.

[8] Du, P,; Schneider, J.; Luo, G.; Brennessel, W. W.; Eisenberg, R. Visible Light-Driven Hydrogen Production from Aqueous Protons Catalyzed by Molecular Cobaloxime Catalysts. *Inorg. Chem.*, **2009**, *48*, 4952–4962.

[9] Zhang, P.; Wang, M.; Li, C.; Li, X.; Dong, J.; Sun, L. Photochemical H_2 Production with Noble-metal-free Molecular Devices Comprising a Porphyrin Photosensitizer and a Cobaloxime Catalyst. *Chem. Commun.*, **2010**, *46*, 8806–8808.

[10] Artero, V.; Chavarot-Kerlidou, M.; Fontecave, M. Splitting Water with Cobalt. *Angew. Chem. Int. Ed.*, **2011**, *50*, 7238–7266.

[11] McKone, J. R.; Marinescu, S. C.; Brunschwig, B. S.; Winkler, J. R.; Gray. H. B. Earth-abundant Hydrogen Evolution Electrocatalysts. *Chem. Sci.*, **2014**, *5*, 865–878.

[12] Queyriaux, N.; Jane, R. T.; Massin, J.; Artero, V.; Chavarot-Kerlidou, M.; Recent Developments in Hydrogen Evolving Molecular Cobalt(II)–Polypyridyl Catalysts. Coord. *Chem. Rev.*, **2015**, 304–305, 3–19.

[13] Coutard, N.; Kaeffer, N.; Artero, V. Molecular Engineered Nanomaterials for Catalytic Hydrogen Evolution and Oxidation. *Chem. Commun.*, **2016**, *52*, 13728–13748.

[14] Dempsey, J. L.; Brunschwig, B. S.; Winkler J. R.; Gray, H. B. Hydrogen Evolution Catalyzed by Cobaloximes. *Acc. Chem. Res.* **2009**, *42*, 1995–2004.

[15] Mulford, K. L.; Utschig, L. M. Modular Homogeneous Chromophore–Catalyst Assemblies. *Acc. Chem. Res.*, **2016**, *49*, 835–843.

[16] Willkomm, J. ; Orchard, K. L. ; Reynal, A. ; Pastor, E. ; Durrant, J. R. ; Reisner, E. Dye-sensitised Semiconductors Modified with Molecular Catalysts for Light-driven H_2 Production. *Chem. Soc. Rev.*, **2016**, *45*, 9–23.

[17] Wood, C. J.; Summers, G. H.; Clark, C. A.; Kaeffer, N.; Braeutigam, M.; Carbone, L. R.; D'Amario, L.; Fan, K.; Farré, Y.; Narbey, S.; Oswald, F.; Stevens, L. A.; Parmenter, C. D. J.; Fay, M. W.; La Torre, A.; Snape, C. E.; Dietzek, B.; Dini, D.; Hammarström, L.;

Pellegrin, Y.; Odobel, F.; Sun, L.; Artero, V.; Gibson, E. A. A Comprehensive Comparison of Dye-Sensitized NiO Photocathodes for Solar Energy Conversion. *Phys. Chem. Chem. Phys.* **2016**, *18*, 10727–10738.

[18]   Xu, P.; McCool, N. S.; Mallouk, T. E. Water Splitting Dye-Sensitized Solar Cells. *Nano Today*, **2017**, *14*, 42–58.

[19]   Brennaman, M. K.; Dillon, R. J.; Alibabaei, L.; Gish, M. K.; Dares, C. J.; Ashford, D. L.; House, R. L.; Meyer, G. J.; Papanikolas, J. M.; Meyer, T. J. Finding the Way to Solar Fuels with Dye-Sensitized Photoelectrosynthesis Cells. *J. Am. Chem. Soc.*, **2016**, *138*, 13085–13102.

[20]   Yu, Z.; Li, F.; Sun, L. Recent Advances in Dye-Sensitized Photoelectrochemical Cells for Solar Hydrogen Production Based on Molecular Components. *Energy Environ. Sci.* **2015**, *8*, 760–775.

[21]   Queyriaux, N.; Kaeffer, N.; Morozan, A.; Chavarot-Kerlidou, M.; Artero, V. Molecular Cathode and Photocathode Materials for Hydrogen Evolution in Photoelectrochemical Devices. *J. Photochem. Photobiol. C* **2015**, *25*, 90–105.

[22]   Gibson, E. A. Dye-Sensitized Photocathodes for H_2 Evolution. *Chem. Soc. Rev.*, **2017**, *46*, 6194–6209.

[23]   Nikolaou, V.; Charisiadis, A.; Charalambidis, G.; Coutsolelos, A. G.; Odobel, F. Recent Advances and Insights in Dye-Sensitized NiO Photocathodes for Photovoltaic Devices. *J. Mater. Chem. A*, **2017**, *5*, 21077–21113.

[24]   Li, L. ; Duan, L. ; Wen, F. ; Li, C. ; Wang, M. ; Hagfeldt, A. ; Sun L. Visible Light Driven Hydrogen Production from a Photo-Active Cathode Based on a Molecular Catalyst and Organic Dye-Sensitized p-Type Nanostructured NiO. *Chem. Commun.*, **2012**, *48*, 988–990.

[25] Kamire, R. J. ; Majewski, M. B. ; Hoffeditz, W. L. ; Phelan, B. T. ; Farha, O. K. ; Hupp, J. T. ; Wasielewski., M. R. Photodriven Hydrogen Evolution by Molecular Catalysts Using Al_2O_3-protected Perylene-3,4-Dicarboximide on NiO Electrodes. *Chem. Sci.*, **2017**, *8*, 541–549

[26] Click, K. A.; Beauchamp, D. R.; Huang, Z.; Chen, W.; Wu, Y. Membrane-Inspired Acidically Stable Dye-Sensitized Photocathode for Solar Fuel Production. *J. Am. Chem. Soc.*, **2016**, *138*, 1174–1179.

[27] Fan, K. ; Li, F. ; Wang, L. ; Daniel, Q. ; Gabrielsson, E. ; Sun, L. Pt-free Tandem Molecular Photoelectrochemical Cells for Water Splitting Driven by Visible Light. *Phys. Chem. Chem. Phys.*, **2014**, *16*, 25234–25240.

[28] Li, F. ; Fan, K. ; Xu, B ; Gabrielsson, E. ; Daniel, Q. ; Li, L. ; Sun, L. Organic Dye-Sensitized Tandem Photoelectrochemical Cell for Light Driven Total Water Splitting. *J. Am. Chem. Soc.*, **2015**, *137*, 9153–9159.

[29] Antila, L. J. ; Ghamgosar, P. ; Maj, S. ; Tian, H. ; Ott, S. ; Hammarström, L. Dynamics and Photochemical H_2 Evolution of Dye–NiO Photocathodes with a Biomimetic FeFe-Catalyst. *ACS Energy Lett.* **2016**, *1*, 1106–1111.

[30] Creissen, C. E. ; Warnan, J. ; Reisner, E. Solar H_2 Generation in Water with a $CuCrO_2$ Photocathode Modified with an Organic Dye and Molecular Ni Catalyst. *Chem. Sci.* **2018**, *9*, 1439−1447.

[31] Kaeffer, N. ; Windle, C. D. ; Brisse, R. ; Gablin, C. ; Leonard, D. ; Jousselme, B. ; Chavarot-Kerlidou, M. ; Artero, V. Insights into the Mechanism and Aging of a Noble-Metal Free H_2-Evolving Dye-Sensitized Photocathode. *Chem. Sci.* **2018**, *9*, 6721-6738.

[32] Gross, M. A. ; Creissen, C. E. ; Orchard K. L. ; Reisner, E. Photoelectrochemical Hydrogen Production in Water using a Layer-by-Layer Assembly of a Ru Dye and Ni Catalyst on NiO. *Chem. Sci.*, **2016**, *7*, 5537−5546.

[33] D. Wang, M. V. Sheridan, B. Shan, B. H. Farnum, S. L. Marquard, B. D. Sherman, M. S. Eberhart, A. Nayak, C. J. Dares, A. K. Das, R. M.Bullock, T. J. Meyer. Layer-by-Layer Molecular Assemblies for Dye-Sensitized Photoelectrosynthesis Cells Prepared by Atomic Layer Deposition. *J. Am. Chem. Soc.* **2017**, *139*, 14518−14525.

[34] Shan, B. ; Sherman, B. D. ; Klug, C. M. ; Nayak, A. ; Marquard, S. L. ; Liu, Q. ; Bullock, R. M. ; Meyer, T. J. Modulating Hole Transport in Multilayered Photocathodes with Derivatized p-Type Nickel Oxide and Molecular Assemblies for Solar-Driven Water Splitting. *J. Phys. Chem. Lett.* **2017**, *8*, 4374−4379.

[35] Shan, B. ; Das, A. K. ; Marquard, S. ; Farnum, B. H. ; Wang, D. ; Bullock, R. M. ; Meyer, T. J.. Photogeneration of Hydrogen from Water by a Robust Dye-Sensitized Photocathode. *Energy Environ. Sci.*, **2016**, *9*, 3693−3697.

[36] Ji, Z. ; He, M. ; Huang, Z. ; Ozkan, U. ; Wu, Y. ; Photostable p-Type Dye-Sensitized Photoelectrochemical Cells for Water Reduction. *J. Am. Chem. Soc.*, **2013**, *135*, 11696–11699.

[37] Kaeffer, N.; Massin, J.; Lebrun, C.; Renault, O.; Chavarot-Kerlidou, M.; Artero, V. Covalent Design for Dye-Sensitized H_2-Evolving Photocathodes Based on a Cobalt Diimine-Dioxime Catalyst. *J. Am. Chem. Soc.* **2016**, *138*, 12308–12311.

[38] Pati, P. B.; Zhang, L.; Philippe, B.; Fernández-Terán, R.; Ahmadi, S.; Tian, L.; Rensmo, H.; Hammarström, L.; Tian, H. Insights into the Mechanism of a Covalently Linked Organic Dye–Cobaloxime Catalyst System for Dye-Sensitized Solar Fuel Devices. *ChemSusChem* **2017**, *10*, 2480– 2495.

[39] Lyu, S.; Farré, Y.; Ducasse, L.; Pellegrin, Y.; Toupance, T.; Olivier, C.; Odobel, F. Push-Pull Ruthenium Diacetylide Complexes: New Dyes for p-Type Dye-Sensitized Solar Cells. *RSC Adv.* **2016**, *6*, 19928–19936.

[40] Massin, J., Lyu, S.; Pavone, M.; Muñoz-García, A; B.; Kaumann, B.; Toupance, T.; Chavarot-Kerlidou, M.; Artero, V.; Olivier, C. Design and Synthesis of Novel Organometallic Dyes for NiO Sensitization and Photo-electrochemical Applications. *Dalton Trans.* **2016**, *45,* 12539–12547.

[41] De Sousa, S.; Ducasse, L.; Kauffmann, B.; Toupance, T.; Olivier, C. Functionalization of a Ruthenium-Diacetylide Organometallic Complex as a Next-Generation Push-Pull Chromophore. *Chem. Eur. J.* **2014**, *20*, 7017–7024.

[42] De Sousa S.; Lyu, S.; Ducasse L.; Toupance T.; Olivier C. Tuning Visible-Light Absorption Properties of Ru-Diacetylide Complexes: a Simple Access to Colorful Efficient Dyes for DSSCs. *J. Mater. Chem. A* **2015**, *3*, 18256–18264.

[43] Olivier, C.; Kim, B.; Touchard, D.; Rigaut, S. Redox-Active Molecular Wires Incorporating Ruthenium(II) σ-Arylacetylide Complexes for Molecular Electronics. *Organometallics* **2008**, *27*, 509–518.

[44] Ruiz Aranzaes, J.; Daniel, M.-C.; Astruc, D. Metallocenes as References for the Determination of Redox Potentials by Cyclic Voltammetry – Permethylated Iron and Cobalt Sandwich Complexes, Inhibition by Polyamine Dendrimers, and the Role of Hydroxy-containing Ferrocenes. *Can. J. Chem.*, **2006**, *84*, 288–299.

[45] Ji, Z.; Wu, Y. Photoinduced Electron Transfer Dynamics of Cyclometalated Ruthenium (II)–Naphthalenediimide Dyad at NiO Photocathode. *J. Phys. Chem. C*, **2013**, 117, 18315-18324.

[46] Queyriaux, N.; Wahyuono, R. A.; Fize, J.; Gablin, C.; Wächtler, M.; Martinez, E.; Léonard, D.; Dietzek, B.; Artero, V.; Chavarot-Kerlidou, M. Aqueous Photocurrent

Measurements Correlated to Ultrafast Electron Transfer Dynamics at Ruthenium Tris Diimine Sensitized NiO Photocathodes. *J. Phys. Chem. C,* **2017**, 121, 5891-5904.

[47] Muñoz-García, A.B.; Pavone, M. Structure and Energy Level Alignment at the Dye-Electrode Interface in p-Type DSSCs: New Hints on the Role of Anchoring Modes from Ab Initio Calculations. *Phys. Chem. Chem. Phys.* **2015**, *17*, 12238–12246.

[48] Kümmel, S. Charge-Transfer Excitations: A Challenge for Time-Dependent Density Functional Theory That Has Been Met. *Adv. Energy Mater.* **2017**, *7*, 1700440.

[49] Ameline, D. ; Diring, S. ; Farre, Y. ; Pellegrin, Y. ; Naponiello, G. ; Blart, E. ; Charrier, B. ; Dini, D. ; Jacquemin, D. ; Odobel, F. Isoindigo derivatives for application in p-type dye sensitized solar cells. *RSC Adv.* **2015**, *5*, 85530–85539.

[50] Grelaud, G.; Gauthier, N.; Luo, Y.; Paul, F.; Fabre, B.; Barrière, F.; Ababou-Girard, S.; Roisnel, T.; Humphrey, M. G. Redox-Active Molecular Wires Derived from Dinuclear Ferrocenyl/Ruthenium(II) Alkynyl Complexes: Covalent Attachment to Hydrogen-Terminated Silicon Surfaces. *J. Phys. Chem. C*, **2014**, 118, 3680–3695.

[51] Mulas, A.; Hervault, Y.-M.; He, X.; Di Piazza, E.; Norel, L.; Rigaut, S.; Lagrost, C. Fast Electron Transfer Exchange at Self-Assembled Monolayers of Organometallic Ruthenium(II) σ-Arylacetylide Complexes. *Langmuir*, **2015**, 31, 7138–7147.

[52] Hoogeveen, D. A.; Fournier, M.; Bonke, S. A.; Nattestad, A.; Mishra, A.; Bäuerle, P.; Spiccia, L.; Mozer, A. J.; Simonov, A. N. Origin of Photoelectrochemical Generation of Dihydrogen by a Dye-Sensitized Photocathode without an Intentionally Introduced Catalyst. *J. Phys. Chem. C* **2017**, *121*, 25836–25846.

[53] Veldkamp, B. S.; Han, W. S.; Dyar, S. M.; Eaton, S. W.; Ratner, M. A.; Wasielewski, M. R. Photoinitiated Multi-Step Charge Separation and Ultrafast Charge Transfer Induced Dissociation in a Pyridyl-linked Photosensitizer–Cobaloxime Assembly. *Energy Environ. Sci.* **2013**, *6*, 1917–1928.

[54] Panagiotopoulos, A.; Ladomenou, K.; Sun, D.; Artero, V.; Coutsolelos, A. G. Photochemical Hydrogen Production and Cobaloximes: the Influence of the Cobalt Axial N-ligand on the System Stability. *Dalton Trans.* **2016**, *45*, 6732–6738.

[55] Kumagai, H.; Sahara, G.; Maeda, K.; Higashi, M.; Abe, R.; Ishitani, O. Hybrid Photocathode Consisting of a CuGaO2 p-Type Semiconductor and a Ru(II)–Re(I) Supramolecular Photocatalyst: Non-biased Visible-light-driven CO_2 Reduction with Water Oxidation. *Chem. Sci.* **2017**, *8*, 4242–4249.

[56] Bakac, A.; Espenson, J. H. Unimolecular and Bimolecular Homolytic Reactions of Organochromium and Organocobalt Complexes. Kinetics and Equilibria. *J. Am. Chem. Soc.*, **1984**, *106*, 5197–5202.

[57] Fulmer, G. R.; Miller, A. J. M.; Sherden, N. H.; Gottlieb, H. E.; Nudelman, A.; Stoltz, B. M.; Bercaw, J. E.; Goldberg, K. I. NMR Chemical Shifts of Trace Impurities: Common Laboratory Solvents, Organics, and Gases in Deuterated Solvents Relevant to the Organometallic Chemist. *Organometallics* **2010**, *29*, 9, 2176–2179.

[58] Gaussian 09, Revision E.01, Frisch, M. J.; Trucks, G. W.; Schlegel, H. B.; Scuseria, G. E.; Robb, M. A.; Cheeseman, J. R.; Scalmani, G.; Barone, V.; Petersson, G. A.; Nakatsuji, H.; Li, X.; Caricato, M.; Marenich, A.; Bloino, J.; Janesko, B. G.; Gomperts, R.; Mennucci, B.; Hratchian, H. P.; Ortiz, J. V.; Izmaylov, A. F.; Sonnenberg, J. L.; Williams-Young, D.; Ding, F.; Lipparini, F.; Egidi, F.; Goings, J.; Peng, B.; Petrone, A.; Henderson, T.; Ranasinghe, D.; Zakrzewski, V. G.; Gao, J.; Rega, N.; Zheng, G.; Liang, W.; Hada, M.; Ehara, M.; Toyota, K.; Fukuda, R.; Hasegawa, J.; Ishida, M.; T. Nakajima, Y. Honda, O. Kitao, H. Nakai, T. Vreven, K. Throssell, J. A. Montgomery, Jr., J. E. Peralta, F. Ogliaro, M. Bearpark, J. J. Heyd, E. Brothers, K. N. Kudin, V. N. Staroverov, T. Keith, R. Kobayashi, J. Normand, K. Raghavachari, A. Rendell, J. C. Burant, S. S. Iyengar, J. Tomasi, M. Cossi, J. M. Millam, M. Klene, C. Adamo, R. Cammi, J. W. Ochterski, R. L.

Martin, K. Morokuma, O. Farkas, Foresman, J. B.; Fox, D. J. Gaussian, Inc., Wallingford CT, **2016.**

[59] Becke, A. D. Density-functional thermochemistry. III. The role of exact exchange. *J. Chem. Phys.* **1993**, *98*, 5648–5652.

[60] Bergner, A.; Dolg, M.; Kuechle, W.; Stoll, H.; Preuss, H. Ab Initio Energy-adjusted Pseudopotentials for Elements of Groups 13–17. *Mol. Phys.* **1993**, *80*, 1431–1441.

[61] Rassolov, V. A.; Ratner, M. A.; Pople, J. A.; Redfern, P. C.; Curtiss, L. A. 6- 31G* Basis Set for Third- row Atoms. *J. Comput. Chem.* **2001**, *22*, 976–984.

[62] Yanai, T.; Tew, D.; Handy, N. A New Hybrid Exchange-Correlation Functional Using the Coulomb-Attenuating Method (CAM-B3LYP). *Chem. Phys. Lett.* **2004**, *393*, 51–57.

[63] Scalmani, G.; Frish, M. J. Continuous Surface Charge Polarizable Continuum Models of Solvation. I. General Formalism. *J. Chem. Phys.* **2010**, *132*, 114110.

Graphic for Table of Content